

Elasticity of microscale volumes of viscoelastic soft matter by cavitation rheometry

Leonid Pavlovsky,¹ Mahesh Ganesan,¹ John G. Younger,² and Michael J. Solomon¹

¹Department of Chemical Engineering, University of Michigan, Ann Arbor, Michigan 48109, USA

²Department of Emergency Medicine, University of Michigan, Ann Arbor, Michigan 48109, USA

(Received 5 June 2014; accepted 4 September 2014; published online 18 September 2014)

Measurement of the elastic modulus of soft, viscoelastic liquids with cavitation rheometry is demonstrated for specimens as small as $1\ \mu\text{l}$ by application of elasticity theory and experiments on semi-dilute polymer solutions. Cavitation rheometry is the extraction of the elastic modulus of a material, E , by measuring the pressure necessary to create a cavity within it [J. A. Zimmerman, N. Sanabria-DeLong, G. N. Tew, and A. J. Crosby, *Soft Matter* **3**, 763–767 (2007)]. This paper extends cavitation rheometry in three ways. First, we show that viscoelastic samples can be approximated with the neo-Hookean model provided that the time scale of the cavity formation is measured. Second, we extend the cavitation rheometry method to accommodate cases in which the sample size is no longer large relative to the cavity dimension. Finally, we implement cavitation rheometry to show that the theory accurately measures the elastic modulus of viscoelastic samples with volumes ranging from 4 ml to as low as $1\ \mu\text{l}$. © 2014 AIP Publishing LLC.

[<http://dx.doi.org/10.1063/1.4896108>]

The linear elastic modulus of a soft material is a mechanical property measurable by techniques such as mechanical rheometry, microrheology, and atomic force microscopy (AFM).^{1,2} Needs for both *in vivo* characterization of linear elasticity (such as in tissue viability) as well as rapid measurement (such as in quality control applications) have driven recent methods development.^{3–5} Mechanical rheometry typically requires approximately milliliter sample volumes and, if sample loading and testing durations are considered, requires as much as 5 min to test one specimen at one deformation frequency. Passive microrheology is a widely used technique to study the mechanical properties of small volumes (between ~ 3 and $50\ \mu\text{l}$) of soft matter. One method of microrheology—which uses the multiple scattering technique of diffusing wave spectroscopy—requires as much as an hour of measurement time. This method can probe elastic moduli up to $\sim 2000\ \text{Pa}$.^{1,6,7} Microrheology measurements can also be impacted by the stability of the dispersed probes and the heterogeneity of the material studied.^{8,9} AFM can also be used to characterize the elastic modulus of very small volumes ($< 1\ \mu\text{l}$) of material; however, this technique requires long durations for measurements and sample preparation time.^{3,10} The duration of these techniques makes them challenging for high throughput applications, while their lack of portability complicates their use as *in vivo* diagnostics.

The cavitation rheometry technique of Zimmerman *et al.* characterizes the linear elastic modulus of soft matter with Young's modulus in the range of $0.12\ \text{kPa} < E < 40\ \text{kPa}$.^{11,12} It is an inexpensive, fast, and portable method that estimates the elastic modulus by measurement of the critical pressure (P_c) required for internal cavitation. Cavitation is induced by air pumped through a needle inserted into the sample. The critical pressure predicts the elastic modulus, E , through the theory of cavitation in an incompressible hyperelastic material.¹¹ A hyperelastic material is described by a rate independent constitutive model that relates the stress to a strain energy density function.¹³ Using a neo-Hookean strain

energy function, the inflation pressure (P), cavity expansion ratio (λ), and the elastic modulus (E) are related by¹⁴

$$\frac{P}{E} = \frac{5 - 4\lambda^{-1} - \lambda^{-4}}{6}. \quad (1)$$

The cavity expansion ratio is the ratio of the radius of the bubble (R_c) formed to the inner diameter of the needle (R_i), $\lambda = R_c/R_i$.¹¹ The critical pressure, P_c , is the maximum inflation pressure, achieved as λ approaches infinity. If the surface tension (γ) of the material is accounted for, the critical pressure is^{11,15}

$$P_c = \frac{5E}{6} + \frac{2\gamma}{R_i}. \quad (2)$$

A linear fit of P_c versus $2/R_i$ yields the elastic modulus.

Two limitations of Eqs. (1) and (2) restrict the scope of this method. The first is that because the analysis assumes a neo-Hookean strain energy function, cavitation rheometry has only been used to characterize materials that are elastic solids.^{11,12,16–19} To extend this method to viscoelastic materials, the assumption of neo-Hookean mechanics must be examined relative to their rheological behavior. The second limitation is that Eqs. (1) and (2) are valid only in the “thick-shell” case of a sample volume whose dimension is large relative to the radius of the expanding cavity.¹⁴ To extend to smaller volumes, the cavitation rheology should be generalized to materials of finite volume. In this paper, we examine these two limitations by theoretical analysis, numerical simulation, and experimental validation. We find that the assumptions that underlie both limitations can be relaxed, allowing cavitation rheometry to be applied to a greater set of materials and a broader range of conditions.

We use semi-dilute solutions of high molar mass poly (ethylene oxide) (PEO, Polysciences, Inc., $1 \times 10^6\ \text{g/mol}$) at 3.0%, 4.0%, 6.0%, and 8.0% (w/w) in water as model materials. In the linear regime, the frequency dependent shear

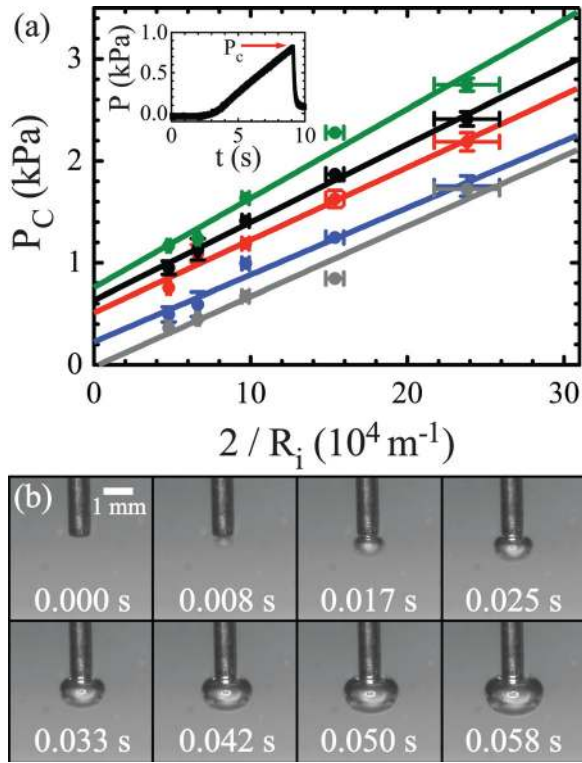


FIG. 1. (a) Critical pressure of PEO solutions and glycerol, as a function of needle size; 3% (blue), 4% (red), 6% (black), 8% (green), and glycerol (grey). Five needle sizes were used (R_i of: 0.084 mm, 0.13 mm, 0.207 mm, 0.302 mm, and 0.419 mm), with three replicates each. The vertical error bars are standard error of the mean and the horizontal error bars are the manufacturer's variability in needle size. Inset: An individual cavitation experiment with 4% PEO and $R_i = 0.419 \text{ mm}$, with P_c denoted as the maximum pressure. (b) Frame-by-frame images of cavitation event 4% PEO with $R_i = 0.084 \text{ mm}$, captured at 120 fps.

elastic ($G'(\omega)$) and viscous ($G''(\omega)$) moduli of these test fluids are plotted in Fig. S1(a) (AR-G2 rheometer, TA Instruments, strain amplitude = 0.3). Because these solutions are incompressible, Poisson's ratio is approximately 0.5 and the elastic and shear moduli are related as $E' = 3G'$.²⁰

The mechanical rheometry (Fig. S1) differs from the behavior of the neo-Hookean constitutive equation in two critical ways: First, a neo-Hookean material is purely elastic, while the polymer solutions display a finite viscous modulus, G'' . Second, in hyperelastic models, the stress-strain relationship is independent of deformation path, strain rate and deformation history.¹⁹ Therefore, the neo-Hookean model describes a frequency-independent elastic modulus, while the polymer solution rheology exhibits frequency-dependent elasticity. We hypothesize that neither of these differences is critical to the application of cavitation rheometry. In the first

case, we show that the viscous contribution to cavitation does not affect the data analysis of Eqs. (1) and (2). In the second case, we show, via imaging, that cavitation occurs at high frequency, at which $G' \sim G''$ or greater. In this limit, the estimate of G' through cavitation rheometry agrees with mechanical rheometry.

The second limitation, the cavitation length scale, must be addressed to extend the technique to small, microliter volumes. The analysis for Eqs. (1) and (2) assumes that cavitation occurs in a region that is small relative to the overall volume of the material. Because the cavitation region scales on the needle radius, the sample volume must be significantly larger than $\sim 0.2 \mu\text{l}$, the minimum volume of material necessary when commercially available needles are used. We hypothesize that, as the sample volume decreases into the microliter range, the thick-wall assumption must be relaxed and Eqs. (1) and (2) must be modified. To verify this second hypothesis, we formulate the elastic analysis for arbitrary volume and validate it by numerical simulation and small volume experiments.

The cavitation pressure of the four test fluids was measured with air as the cavitating agent, delivered at 0.4 ml/min via syringe pump (Fisher Scientific). To differentiate the viscoelastic response from that of a purely viscous fluid, experiments were also performed on glycerol. Cavitation was induced with five needle radii from 0.084 mm to 0.419 mm (Hamilton). The specimen volume was greater than 1 ml, a limit in which Eq. (2) applies. The time for cavitation was $\sim 10 \text{ s}$. Once initiated, cavity formation was rapid, typically $< 80 \text{ ms}$. The cavitation pressure is the maximum pressure observed.

Fig. 1(a) yields the shear elastic modulus from the intercept (i.e., it is $2/5$ of the intercept) and γ from the slope of the fit. The cavitation of glycerol (gray) results in $G' = 0$, within error. This result demonstrates an inelastic fluid can be identified as such by the technique. The error for glycerol provides a lower bound on the G' resolution limit of cavitation rheometry. Specifically, the $\sim 50 \text{ Pa}$ error in the intercept for glycerol indicates that a G' of this magnitude or lower cannot be resolved. These values and standard errors of the mean are in Table I.

We compare the moduli to those determined from mechanical rheometry. We performed high-speed imaging of the cavity formation (Fig. 1(b)). From these images, we estimate a characteristic strain rate for cavitation at which mechanical and cavitation rheometry are compared. Images were acquired with a CCD camera at 120 frames per second (Pulnix Progressive Scan TM-6710) attached to a $20\times$ stereoscope (Zeiss Stemi 2000-C). From the imaging, seen

TABLE I. The shear elastic modulus and surface tension from cavitation curves of Figure 1(a) compared to the modulus from mechanical rheometry at a strain rate estimated from high-speed imaging. The total strain to cavitation and correction factor is also reported. The rheometry values for the 3% PEO sample were not evaluated due to limitations of the camera frame rate.

Test material	Rheometry G' (Pa)	Cavitation G' (Pa)	Correction factor, k	Total strain, ϵ	Characteristic strain rate, $\dot{\epsilon}$ (s^{-1})	Surface tension, (N/m)
3% PEO	...	91 ± 33	0.066 ± 0.006
4% PEO	140	205 ± 31	0.70 ± 0.11	1.80	270	0.071 ± 0.006
6% PEO	290	255 ± 20	1.1 ± 0.09	0.65	130	0.077 ± 0.004
8% PEO	590	305 ± 47	1.9 ± 0.30	0.21	74	0.088 ± 0.008
Glycerol	...	-8 ± 48	0.069 ± 0.009

frame-by-frame for a 4% PEO solution in Fig. 1(b), we measured the bubble radius for each frame of cavity growth using image processing software (ImageJ). The local strain, ε_L , and the strain rate, $\dot{\varepsilon}$, were determined at each frame as $\varepsilon_L = (R_j - R_{j-1})/R_{j-1}$ and $\dot{\varepsilon} = \varepsilon_L/t_c$, where t_c is the time between frames j and $j-1$. The point of maximum strain rate was designated the critical condition for cavitation. The total strain, ε , was determined from the beginning of the experiment to the point of cavitation as $\varepsilon = (R_{j,\text{critical}} - R_i)/R_i$. The cavitation rate varied from 74 s^{-1} (8% PEO) to 270 s^{-1} (4% PEO) for the cavitation pressures and surface tensions listed in Table I. By means of the Cox-Merz rule, we compare G' at the cavitation rate to $G'(\omega)$ at the equivalent frequency from the mechanical rheology.²¹

The shear elastic moduli at the aforementioned frequencies are in a region at which $G' \sim G''$ and the elasticity of the system is significant. This correlation validates our first hypothesis and therefore, we directly compare the cavitation and mechanical rheometry at these deformation rates.

We establish a correction factor, $k = G'_{\text{Rheo}}/G'_{\text{Cav}}$ to connect cavitation and mechanical rheometry. We find that the average correction factor ($k_{\text{avg}} = 1.23 \pm 0.17$) results in a cavitation rheometry deviation from the mechanical rheometry modulus that is not more than a factor of two. Although cavitation and mechanical rheometry agree to within a factor of two and both sets of moduli increase with increasing PEO, the dependence of each displays a different dependence of PEO concentration. This result is likely tied to the sensitivity of the comparison to the strain rate extracted from imaging; additional experimental and theoretical effort to improve this comparison is warranted. Nevertheless, the cavitation and mechanical rheometry results differ, on average, by less than a factor of two. Although not exact, this accuracy would be acceptable for many applications. For example, the difference in G' between healthy tissue and a cancerous tumor is approximately an order of magnitude or greater.⁴

Table I also indicates that the liquid-air γ of the solutions increases modestly with PEO concentration. The γ of PEO solutions should be bounded 0.043 N/m and 0.072 N/m, the values for PEO and pure water, respectively.²²⁻²⁴ A value closer to water is expected because the polymers in solution have yet to diffuse to the freshly created interface.^{25,26} There is also the additional effect of finite viscosity, as discussed in the supplementary material (Fig. S3).³¹ Although this effect vanishes in the limit used to characterize the elastic modulus, it may affect γ characterization, and thereby be a determinant of the values and errors discussed.

We now address the second, volumetric, limitation of cavitation rheometry. The “thick-shell” assumption in Eqs. (1) and (2) takes the deformation due to cavitation to be local and contained within an infinitesimal volume surrounding the needle.²⁷ The outer boundary of the specimen is sufficiently far from the needle and therefore unperturbed by cavitation deformation. However, with decreasing sample volume, the outer boundary approaches the radius of the expanding cavity, which creates a deformation field extending to the outer boundary (cf. supplementary material).³¹

To study these mechanics, we performed finite element simulations (COMSOL Multiphysics) of cavitation in finite volumes of a neo-Hookean material with internal loading

and unconstrained radial expansion of the outer boundary,²⁸ details of which can be found in the supplementary material.³¹ The volume of material was varied through the thickness of the elastic shell, H . The pressure curves found from simulation (Fig. 2 Inset) are plotted as P/E as a function R_c/R_i , where R_c is the cavity radius. The response is dependent on the amount of material initially present (i.e., $(R_i + H)/R_i$, where $R_i + H$ is the radius of the specimen). At small material volumes ($(R_i + H)/R_i \leq 5$), after reaching its critical value, the pressure decreases with increasing cavity expansion. This effect physically would be manifested as an unbounded expansion at this critical pressure.¹³ For $(R_i + H)/R_i > 5$, the critical pressure increases and occurs at increasingly larger values of R_c/R_i . At large volumes, such as $(R_i + H)/R_i = 20$, the pressure reaches an asymptotic limit of $\sim 5E/6$, consistent with Eq. (2). The critical pressure is significantly lower for finite volumes (i.e., $P_c \sim 0.5E$ and $\sim 0.2E$ at $(R_i + H)/R_i$ equal to 5 and 1.5, respectively). This difference indicates that applying Eq. (2) in this regime is not valid.

We analyzed the mechanics of cavity deformation in a neo-Hookean material. The material is defined as a hollow sphere of internal radius, R_i , and an external radius, $R_i + H$, which is free to expand. Assuming incompressibility, the application of a pressure at the inner wall generates equibiaxial extension.²⁷ Upon solving the equilibrium momentum balance subject to the boundary conditions of internal loading and an unbounded surface, we find that the applied pressure, P , and deformation, λ , are related as

$$P = \frac{E}{6\lambda_b^4} + \frac{2E}{3\lambda_b} - \frac{E}{3} \left(\frac{1}{2\lambda^4} + \frac{2}{\lambda} \right). \quad (3)$$

Here, λ is the spatially varying stretch ratio of the cavity and λ_b is the stretch ratio of the material at any point within the elastic shell. Additional details are found in the supplementary material.³¹ By numerically solving Eq. (3) and comparing to simulations, we find that the theory curve overlays exactly with the simulation results (Fig. 2 Inset). Furthermore, we numerically generate pressure-stretch curves to determine P_c at many dimensionless sample

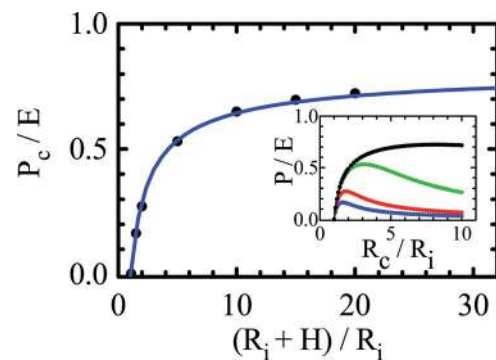


FIG. 2. The dependence of normalized critical pressure (P_c/E) on the volume ratio of material as from finite element analysis (black circles) and theory (blue line). These results were fit with Eq. (4) to determine parameters a and b . Inset: Simulation and theory of normalized pressure versus normalized cavity radius (R_c/R_i) during inflation. The curves are for $[R_i + H]/R_i$ of 1.5 (blue), 2.0 (red), 5.0 (green), and 20.0 (black).

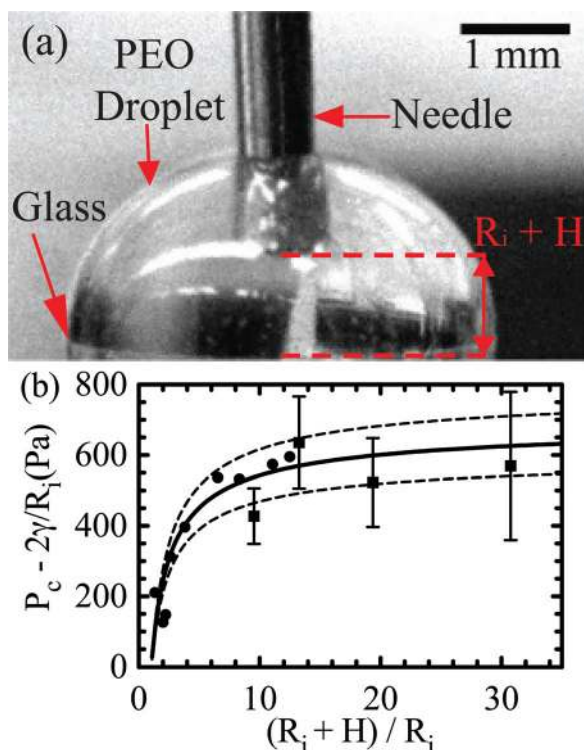


FIG. 3. (a) Image of $\sim 1 \mu\text{l}$ droplet of 4% PEO solution on a hydrophobic glass slide for small volume cavitation. The needle and characteristic dimension, $R_i + H$, are shown. (b) P_c , with the surface tension contribution subtracted, plotted for a range of drop dimensions. Small (circles) and large (squares) volume cavitation experiments are plotted and fit (solid line) with Eq. (4). The 95% confidence interval (dotted lines) are shown.

thicknesses. From these calculated values, we obtain the modified cavitation equation by fitting the results (Fig. 2) to

$$P_c = \frac{5E}{6} \left[\frac{6a}{5} \left(\frac{R_i + H}{R_i} \right)^b + 1 \right], \quad (4)$$

where a and b are fitting parameters, equal to -0.8558 and -0.6547 , respectively. Under the limit of infinite material volume ($(R_i + H)/R_i \rightarrow \infty$), Eq. (4) approaches Eq. (2) monotonically, thus validating our fit. This equation is valid for all $H > 0$, as $R_i + H > R_i$.

Equation (4) predicts that the cavitation pressure in finite volumes is a function of the elastic modulus and the geometric parameter $(R_i + H)/R_i$. To test this equation in the finite volume limit, 4% PEO droplets of varying volume were dispensed on a glass slide. To cause the PEO droplet to bead, the glass was coated with a hydrophobic layer (Rain-X). The droplet dimensions were measured with a stereoscope equipped with a CCD camera (PCO Pixelfly QE). The overall volume of our PEO droplets were approximately $1 \mu\text{l}$.

Cavitation was induced in the small volume drops by pressurization of the syringe. The measured cavitation pressures, after subtracting the surface tension term as determined by large volume cavitation ($2\gamma/R_i$), are plotted for a range of drop dimensions in Fig. 3(b). The trend between the small volume (circles) and large volume experiments (squares) is consistent with both the simulation and theory reported earlier. The small volume experiments were fit with Eq. (4), which yielded an elastic modulus of 840 Pa. The

large volume experiments, from Table I, found $E = 615 \text{ Pa}$, a discrepancy of 35%. Moreover, the large volume data fell within the 95% confidence interval of our small volume fitting, further indicating the applicability of Eq. (4).

In conclusion, cavitation rheometry has been extended to estimate the elastic modulus of viscoelastic fluids and small volumes. Areas for future attention include viscoelastic modeling of the cavitation experiment; this step would allow correspondence between this technique and other methods for elongation deformation, and their accompanying instabilities, to be better assessed.^{29,30} These extensions improve the scope for the method's application to areas such as *in situ* and high throughput rheology.

This work was supported by the NSF CDI Program (Grant No. PHYS-0941227), the NIGMS (Grant No. GM-069438), and a University of Michigan Rackham Merit Fellowship (to L.P.). We thank Professor M. A. Burns for use of the high-speed camera.

- ¹P. Cicutta and A. M. Donald, *Soft Matter* **3**, 1449 (2007).
- ²N. Gavara and R. Chadwick, *Nat. Nanotechnol.* **7**, 733 (2012).
- ³M. Balooch, I. C. Wu-Magidi, A. Balazs, A. S. Lundkvist, S. J. Marshall, G. W. Marshall, W. J. Siekhaus, and J. H. Kinney, *J. Biomed. Mater. Res.* **40**, 539 (1998).
- ⁴W.-C. Yeh, P.-C. Li, Y.-M. Jeng, H.-C. Hsu, P.-L. Kuo, M.-L. Li, P.-M. Yang, and P. H. Lee, *Ultrasound Med. Biol.* **28**, 467 (2002).
- ⁵L. Pavlovsky, J. G. Younger, and M. J. Solomon, *Soft Matter* **9**, 122 (2013).
- ⁶T. G. Mason and D. A. Weitz, *Phys. Rev. Lett.* **74**, 1250 (1995).
- ⁷Q. Lu and M. J. Solomon, *Phys. Rev. E* **66**, 061504 (2002).
- ⁸T. M. Squires and T. G. Mason, *Annu. Rev. Fluid Mech.* **42**, 413 (2010).
- ⁹T. Savin and P. S. Doyle, *Biophys. J.* **88**, 623 (2005).
- ¹⁰N. Jalili and K. Laxminarayana, *Mechatronics* **14**, 907 (2004).
- ¹¹J. A. Zimmerlin, N. Sanabria-DeLong, G. N. Tew, and A. J. Crosby, *Soft Matter* **3**, 763–767 (2007).
- ¹²J. A. Zimmerlin, J. J. McManus, and A. J. Crosby, *Soft Matter* **6**, 3632 (2010).
- ¹³R. W. Ogden, *Non-linear Elastic Deformations* (Halsted Press, New York, 1984), p. 532.
- ¹⁴A. N. Gent, *Int. J. Non Linear Mech.* **40**, 165 (2005).
- ¹⁵A. N. Gent and D. A. Tompkins, *J. Appl. Phys.* **40**, 2520 (1969).
- ¹⁶J. A. Zimmerlin and A. J. Crosby, *J. Polym. Sci., Part B: Polym. Phys.* **48**, 1423 (2010).
- ¹⁷A. Delbos, J. Cui, S. Fakhouri, and A. J. Crosby, *Soft Matter* **8**, 8204 (2012).
- ¹⁸S. Kundu and A. J. Crosby, *Soft Matter* **5**, 3963 (2009).
- ¹⁹L. R. G. Treloar, *The Physics of Rubber Elasticity*, 3rd ed. (Oxford University Press, New York, 2005).
- ²⁰J. D. Ferry, *Viscoelastic Properties of Polymers*, 3rd ed. (John Wiley & Sons, New York, 1980), p. 641.
- ²¹C. W. Macosko, *Rheology: Principles, Measurements, and Applications* (Wiley-VCH, Inc., New York, 1994), p. 550.
- ²²R.-J. Roe, *J. Phys. Chem.* **72**, 2013 (1968).
- ²³A. K. Rastogi and L. E. St. Pierre, *J. Colloid Interface Sci.* **35**, 16 (1971).
- ²⁴J. A. Dean, *Lange's Handbook of Chemistry*, 15th ed. (McGraw-Hill Professional, 1998), p. 1424.
- ²⁵N. J. Alvarez, L. M. Walker, and S. L. Anna, *Langmuir* **26**, 13310 (2010).
- ²⁶J. Eastoe and J. S. Dalton, *Adv. Colloid Interface Sci.* **85**, 103 (2000).
- ²⁷A. E. Green and W. Zerna, *Theoretical Elasticity*, 2nd ed. (Dover Publications, Inc., Mineola, 2012).
- ²⁸G. A. Holzapfel, *Nonlinear Solid Mechanics: A Continuum Approach for Engineering* (John Wiley & Sons, New York, 2000), p. 470.
- ²⁹G. H. McKinley and O. Hassager, *J. Rheol.* **43**, 1195 (1999).
- ³⁰A. Y. Malkin and C. J. S. Petrie, *J. Rheol.* **41**, 1 (1997).
- ³¹See supplementary material at <http://dx.doi.org/10.1063/1.4896108> for details about the mechanical rheometry of PEO, the effects of viscosity on cavitation rheometry, the finite element simulations, and the derivations of the volume-dependent cavitation equation.